A&A 640, A38 (2020)
https://doi.org/10.1051/0004-6361/202038156

Astronomy & Astrophysics

Morphology and surface photometry of a sample of isolated early-type galaxies from deep imaging*

R. Rampazzo[1], A. Omizzolo[2,5], M. Uslenghi[3], J. Román[4], P. Mazzei[5], L. Verdes-Montenegro[4], A. Marino[5], and M. G. Jones[4]

[1] INAF Osservatorio Astronomico di Padova, Via dell'Osservatorio 8, 36012 Asiago, Italy
e-mail: roberto.rampazzo@inaf.it
[2] Vatican Observatory, Vatican City
e-mail: aomizzolo@specola.va
[3] INAF-IASF, Via A. Curti 12, 20133 Milano, Italy
e-mail: michela.uslenghi@inaf.it
[4] Dep.to Astronomia Extragaláctica Istituto Astrofisica de Andalucía, Glorieta de la Astronomia s/n, 18008 Granada, Spain
[5] INAF Osservatorio Astronomico di Padova, Vicolo dell'Osservatorio 5, 35122 Padova, Italy

Received 13 April 2020 / Accepted 22 May 2020

ABSTRACT

Context. Isolated early-type galaxies are evolving in unusually poor environments for this morphological family, which is typical of cluster inhabitants. We investigate the mechanisms driving the evolution of these galaxies.
Aims. Several studies indicate that interactions, accretions, and merging episodes leave their signature on the galaxy structure, from the nucleus down to the faint outskirts. We focus on revealing such signatures, if any, in a sample of isolated early-type galaxies, and we quantitatively revise their galaxy classification.
Methods. We observed 20 (out of 104) isolated early-type galaxies, selected from the AMIGA catalog, with the 4KCCD camera at the Vatican Advanced Technology Telescope in the Sloan Digital Sky Survey g and r bands. These are the deepest observations of a sample of isolated early-type galaxies so far: on average, the light profiles reach $\mu_g \approx 28.11 \pm 0.70$ mag arcsec^{-2} and $\mu_r \approx 27.36 \pm 0.68$ mag arcsec^{-2}. The analysis was performed using the AIDA package, providing point spread function-corrected 2D surface photometry up to the galaxy outskirts. The package provides a model of the 2D galaxy light distribution, which after model subtraction enhances the fine and peculiar structures in the residual image of the galaxies.
Results. Our re-classification suggests that the sample is composed of bona fide early-type galaxies spanning from ellipticals to late-S0s galaxies. Most of the surface brightness profiles are best fitted with a bulge plus disc model, suggesting the presence of an underlying disc structure. The residuals obtained after the model subtraction show the nearly ubiquitous presence of fine structures, such as shells, stellar fans, rings, and tails. Shell systems are revealed in about 60% of these galaxies.
Conclusions. Because interaction, accretion, and merging events are widely interpreted as the origin of the fans, ripples, shells and tails in galaxies, we suggest that most of these isolated early-type galaxies have experienced such events. Because they are isolated (after 2–3 Gyr), these galaxies are the cleanest environment in which to study phenomena connected with events like these.

Key words. galaxies: elliptical and lenticular, cD – galaxies: photometry – galaxies: interaction – galaxies: evolution

1. Introduction

Since the discovery of the morphology-density relation, early-type galaxies (Es + S0s = ETGs hereafter) have been known to be typical inhabitants of dense clusters (Dressler 1980; Houghton 2015). Although with the large uncertainty introduced by automatic galaxy classifications, studies based on the Sloan Digital Sky Survey (SDSS; see e.g. York 2000; Abazajian et al. 2009) have shown that ETGs represent a minority (≈10% E and ≈20% S0s) of the galaxy population in the lowest density fields (see e.g. Goto et al. 2003, their Fig. 12). One of the pioneering attempts to characterise the population of galaxies in relatively high isolation produced the Catalog of Isolated Galaxies in the Northern Hemisphere by Karachentseva (1973), which includes a small set of isolated ETGs (iETGs hereafter). Several catalogues of isolated galaxies have been produced since then (e.g. Verdes-Montenegro et al. 2005; Hernández-Toledo et al. 2010; Argudo-Fernàndez et al. 2013, 2015). Historically, these efforts are intended to provide the best sample of unperturbed galaxies to be used as a baseline for comparison of galaxy properties with interacting or cluster samples, for example (see e.g. Rampazzo 2016).

The study of the evolutionary scenario that gives rise to iETGs is of particular interest because their environment is so unusual for this class of galaxy. ETGs are thought to be the final product of the galaxy evolution, where different phenomena, from secular to accretion driven, can play a role (Cappellari 2016). Simulations suggest that interaction, accretion and merging episodes (see Eliche-Moral et al. 2018; Mazzei et al. 2019, and references therein) leave their signatures on galaxies, from the nuclear cuspy versus core shape (Lauer et al. 1991, 1992; Lauer 2012; Côté et al. 2006; Turner et al. 2012) to their outskirts, where tails, streams, fans, and shells may be found (Arp 1966; Malin & Carter 1983; Prieur 1988; Wilkinson et al. 2000; Duc et al. 2015). Shells are often found in ETGs. They are described as interleaved stellar tidal debris with large opening angles and low surface brightness that are often situated on either

* The reduced images are only available at the CDS via anonymous ftp to cdsarc.u-strasbg.fr (130.79.128.5) or via http://cdsarc.u-strasbg.fr/viz-bin/cat/J/A+A/640/A38

side of the galaxy centre and have regular as well as irregular shapes (Dupraz & Combes 1987; Weil & Hernquist 1993; Pop et al. 2018; Mancillas et al. 2019). These signatures have different lifetimes and originate from different mechanisms. Recently, Mancillas et al. (2019) pointed out that tails emerge from the primary galaxy and streams are generated from the secondary galaxy. Tails have shorter lifetimes (2 Gyr) than shells. Shells are generated by minor and major either wet or dry mergers and are long lasting (3 Gyr) (see also Dupraz & Combes 1987; Weil & Hernquist 1993; Longhetti et al. 1999). Streams remains visible in all phases of galaxy evolution.

For iETGs, the detection of these fine structures may help to understand the time that elapsed from their last interaction, accretion, and merging episode. In general, ETGs in low-density environments are found to be rejuvenated in their centre as well as in their outskirts, as shown by the Galaxy Evolution Explorer (GALEX; Martin et al. 2006), suggesting that some form of activity might be induced by interaction, accretion, and merging episodes (Clemens et al. 2006, 2009; Schawinski et al. 2007; Rampazzo et al. 2007; Marino et al. 2011a,b; Mazzei et al. 2014a,b, 2019; Mapelli et al. 2015; Hagen et al. 2016, and references therein).

The SDSS has widely contributed to the investigation of iETGs. Many studies have been dedicated to a visual reclassification of the galaxies in the Karachentseva (1973) catalog and/or revisions of it (Sulentic et al. 2006; Fernandez-Lorenzo et al. 2012; Buta et al. 2019). Hernández-Toledo et al. (2008; H-T hereafter) performed a study (using DR6) of the 579 galaxies in the Karachentseva (1973) sample, including iETGs (58 E, 14 E/S0, 67 S0, and 19 S0/a). They revised the ETG classification on the basis of the geometric profiles obtained by r-band images using `IRAF` (Jedrzejewski 1987). This process classified only 18 galaxies (3.5% of the entire sample) as bona fide E. They are listed in their Table 6. The authors report a 50% incidence of ripples and shells in these Es (9 out of 18), see Table 6 of the paper, although 4 are uncertain detections) as well as a high fraction of Es with diffuse halo (7 out of 18). Recently, Rampazzo et al. (2019) found interaction and merging signatures in a high spatial resolution study in K band, performed with `ARGOS+LUCI` at the Large Binocular Telescope (LBT; Rabien et al. 2019), of KIG 685 and KIG 895. This latter has been found to be a misclassified spiral with a tail. KIG 685 is a bona fide ETG with shells that would suggest an eventful life like that of ETGs in loose galaxy associations, where shells, for instance, are found with a higher frequency than in clusters (see e.g. Malin & Carter 1983; Reduzzi et al. 1996).

The above studies emphasised two aspects. The first aspect is the lack of a quantitative classification of the morphology of isolated galaxies, in particular, of iETGs whose classification is still very uncertain (cf. Sect. 2). For example, H-T found that E+S0 make up 8.5% (3.5% + 5%) of E + S0 + E/S0 (5.7% + 6.6% + 1.4%), while Sulentic et al. (2006) found them to make up 13.7%. The other aspect is that we need surface photometric studies that are deep enough to reveal the fine structure of iETGs, if any. These considerations motivated the present study. Using g and r deep surface photometry, we search for such faint features in iETGs and refine the previously proposed iETG galaxy morphological classification (Sulentic et al. 2006; Fernandez-Lorenzo et al. 2012; Buta et al. 2019) by substantiating the view of H-T about the rarity of Es versus S0s in samples of isolated galaxies. This will help understand their evolutionary mechanisms and the meaning of their current relative isolation.

The paper is structured as follows. The observed sample is presented in Sect. 2. In Sect. 3 we present the observations performed at the Vatican Advanced Technology Telescope (VATT) with the 4K CCD camera. This section also describes the reduction method we implement that fully exploits the quality of the observations. Results are presented in Sect. 4. In Sect. 5 we discuss our results to understand the nature and evolutionary paths of our iETGs.

2. The sample

The sample set is composed of 20 iETGs that are included in the Analysis of the interstellar Medium of Isolated Galaxies sample (AMIGA, Verdes-Montenegro et al. (2005)), which is a revision of the 1973 catalogue of Karachentseva (1973). The analysis of the AMIGA sample revealed a set of galaxies that should not have interacted for at least 3 Gyr (Verdes-Montenegro et al. 2005; Verley et al. 2007a,b).

2.1. The iETGs classification problem

In addition to the morphological classification, we selected the sample by considering the galaxy observability (see Sect. 3). We selected galaxies using the classification of Fernandez-Lorenzo et al. (2012), which is an updated version of the Sulentic et al. (2006) classification. For comparison, we also considered the classification provided by `HyperLeda` and the recent morphological classification by Buta et al. (2019). We collect in Table 1 and Table 2 the classifications and the main galaxy characteristics. In the results section (Sect. 4) we also consider the classification of H-T, which is based on the geometrical profiles of the galaxies.

The differences among the classifications are summarised in Fig. 1. The morphological type distribution, provided by Fernandez-Lorenzo et al. (2012), ranges from $-5 \leq T \leq 0$, that is, it covers the entire range of iETGs, and contains a large portion of galaxies with a disc component ($-3 < T < 0$). However, we note that the galaxy morphological classification is often (largely) discordant among these authors, as shown in Table 1 and Fig. 1. Some galaxies, that is, KIG 481 and KIG 620, are late type ($T > 0$) according to Buta et al. (2019), and KIG 620, KIG 644, and KIG 733, which are all seen edge-on, are classified as late type by `HyperLeda`.

Buta et al. (2019), who most recently classified our iETGs visually, on average tend to provide earlier $\Delta T = -0.5$ morphological type than both `HyperLeda` and Fernandez-Lorenzo et al. (2012). These latter classifications differ by $\Delta T = 0.05$ on average, but single cases may differ more significantly, as shown in the middle panel of Fig. 1. We here quantitatively verify the classification using surface photometry, for example, by determining the presence of a disc. Out of 20 ETGs, 5 show peculiarities (pec) according to the Buta et al. (2019) classification: KIG 481, KIG 490, KIG 685, KIG 733, and KIG 841.

The heliocentric velocity of only two objects is lower than 3000 km s^{-1}. These are KIG 481 and KIG 637. The average heliocentric velocity is $V_{\rm hel} = 8535$ km s^{-1} (Table 1). Distances are taken from Jones et al. (2018), who analysed the AMIGA sample in HI. They used the Mould et al. (2000) model for distances. This model corrects for Local Group motion and uses separate attractor velocity fields for the Virgo cluster, the Shapley supercluster, and the Great Attractor. The distance is finally obtained by adopting $H_0 = 70$ km s^{-1} Mpc^{-1}. The relevant photometric properties of iETGs are collected in Table 2. The g and r photometric data sets are taken from the SLOAN (CModel) values reported in `NED`. The GALEX near-UV (NUV hereafter) integrated magnitudes are also taken from `NED`.

2.2. Degree of isolation in the sample

The environment of the AMIGA galaxies was investigated to avoid similar size companions. Different criteria were developed

Table 1. Sample: KIGs morphology, heliocentric velocity, and adopted distance.

KIG	RA J2000	Dec. J2000	Buta	Morphology (type) HyperLeda	F-L+	V_{hel} [km s^{-1}]	D [Mpc]
264	08 36 01.5	+30 15 59	SB0$^-$(−3.0)	SB0-a (−0.7 ± 1.6)	E/S0 (−3.0 ± 1.5)	7715 ± 26	113.9 ± 4.4
378	09 51 28.1	+10 55 12	E2 (−5.0)	E (−5.0 ± 2.0)	E/S0 (−3.0 ± 1.5)	10385 ± 54	153.8 ± 5.4
412	10 24 46.4	+46 27 22	E1 (−5.0)	E (−5.0 ± 2.0)	E (−4.0 ± 1.5)	12789 ± 120	187.1 ± 6.1
481	11 27 41.2	+66 35 23	SA(l,rs)a pec/E-S0 pec (1.0)	S0-a (−0.1 ± 0.5)	S0 (−2.0 ± 1.5)	1608 ± 16	28.0 ± 3.0
490	11 36 39.6	+06 17 31	SA(r$\bar{s}$:)0/a pec (0.0)	S0(r) (−1.1 ± 0.9)	S0 (−2.0 ± 1.5)	5700 ± 36	89.4 ± 4.0
517	12 02 52.1	+26 15 10	E3 (−5.0)	S0 (−2.2 ± 1.3)	S0 (−2.0 ± 1.5)	9633 ± 30	144.0 ± 5.1
578	13 16 15.4	+20 02 52	E1 (−5.0)	E (−5.0 ± 2.0)	E (−4.0 ± 1.5)	9191 ± 18	139.5 ± 5.0
595	13 39 11.6	+61 30 22	E4-5 (−5.0)	E (−4.8 ± 0.6)	S0 (−2.0 ± 1.5)	9406 ± 53	139.6 ± 5.0
599	13 48 34.6	+37 06 48	SA0$^-$(−3.0)	(R)S0 (−2.3 ± 1.7)	S0/a (0.0 ± 1.5)	10248 ± 17	153.6 ± 5.4
620	14 13 49.2	+37 16 09	SA($\bar{r}$l)0/$\bar{a}$:/E(d)2 (0.5)	SBa (1.0 ± 1.6)	S0 (−2.0 ± 1.5)	6621 ± 29	102.2 ± 4.1
636	14 33 31.4	+57 42 42	SAB(l:)0^{-0} (−2.5)	SB0 (−2.0 ± 2.0)	E/S0 (−3.0 ± 1.5)	11238 ± 58	165.8 ± 5.6
637	14 34 52.4	+54 28 33	E4 (−5.0)	E-S0 (−3.2 ± 1.0)	E (−4.0 ± 1.5)	2119 ± 59	37.4 ± 3.1
644	14 43 54.7	+43 34 50	SAB$\bar{x}$a(r)0$^+$ (−1.0)	(R)Sab (2.2 ± 1.8)	S0/a (0.0 ± 1.5)	8117 ± 30	122.9 ± 4.6
670	15 19 30.2	+67 30 17	E3-4 (−5.0)	E/S0 (−3.0 ± 1.7)	S0 (−2.0 ± 1.5)	12477 ± 35	183.2 ± 6.1
685	15 30 15.2	+56 49 56	E$^+$0: pec (−4.0)	E (−3.9 ± 2.4)	E/S0 (−3.0 ± 1.5)	15383 ± 150	224.5 ± 7.1
705	15 47 44.4	+37 12 18	E$^+$0 (−4.0)	E-S0 (−3.5 ± 2.1)	E (−4.0 ± 1.5)	11947 ± 72	172.2 ± 5.9
722	16 08 32.7	+09 36 24	E/E$^+$1 (−4.5)	E (−4.0 ± 1.8)	E (−4.0 ± 1.5)	10238 ± 31	154.1 ± 5.3
732	16 16 52.	+53 00 22	E/E$^+$1 (−4.5)	E (−4.9 ± 0.6)	E (−4.0 ± 1.5)	5615 ± 31	86.3 ± 3.8
733	16 17 56.9	+22 56 44	(R1P)SAB(s)0/a pec (0.0)	SABa (1.5 ± 2.1)	S0/a (0.0 ± 1.5)	4512 ± 32	72.2 ± 3.6
841	17 59 14.7	+45 53 13	SA(rpl)0/s pec (0.0)	E-S0 (−3.0 ± 0.5)	S0/a (0.0 ± 1.5)	5763 ± 55	87.6 ± 3.8

Notes. Classifications are from Buta et al. (2019) (Col.4), HyperLeda (Col. 5), and Fernandez-Lorenzo et al. (2012) (F-L+ Col. 6). The heliocentric velocity (Col. 7) is from NED and the distance (Col. 8) is taken from Jones et al. (2018) (see Sect. 2).

to define the isolation parameters (Verley et al. 2007a; Argudo-Fernàndez et al. 2013, 2015). Fig. 2 shows the isolation parameters of the 114 iETGs in the AMIGA sample classified by Fernandez-Lorenzo et al. (2012), devised by Verley et al. (2007a). Verley et al. (2007a) calculated the η_K and $Q_{\rm Kar}$ parameters by defining the local galaxy number density and the distribution of the tidal strength, respectively. According to the Verley et al. (2007a) parameters, the four galaxies KIG 412, KIG 595, KIG 644, and KIG 637 are located outside the fiducial range in the Q versus η_k plane for isolated galaxies (dashed horizontal and vertical lines in Fig. 2).

More recently, Argudo-Fernàndez et al. (2013) further revised the isolation criteria of the AMIGA galaxies using both photometric and spectroscopic data from SDSS to refine the η_K and $Q_{\rm Kar}$ parameters. Of the iETGs in this work, Argudo-Fernàndez et al. (2013) found that only KIG 599 is considered isolated when the original isolation criteria of Karachentseva (1973) are applied to SDSS images. However, most of the iETGs pass the criteria for the (photometric) tidal interaction and neighbour density parameters recommended by Argudo-Fernàndez et al. (2013), $Q_{\rm Kar} < -2$ and $\eta_K < 2.7$, meaning that they are assumed to be minimally affected by any neighbours. The exceptions are KIG 517, KIG 644, KIG 722, and KIG 733, all of which violate the neighbour density criterion, but not the tidal interaction criterion. In their spectroscopic analysis, Argudo-Fernàndez et al. (2013) found that about half of the iETG sample do fulfil the Karachentseva isolation criteria when neighbours separated by more than 500 km s^{-1} from the target (in redshift) are removed. This includes KIG 644 and KIG 733, which did not pass the photometric criteria. The galaxies that fail are KIG 264, KIG 517, KIG 595, KIG 620, KIG 637, and KIG 722. There are no measurements (photometric or spectroscopic) for KIG 481, KIG 670, or KIG 732, and KIG 841 lacks spectroscopic measurements. In the cases of KIG 412 and KIG 644, Argudo-Fernàndez et al. (2013) is at odds with Verley et al. (2007a) because they did not meet the previous criteria. When they used the spectroscopic data, Argudo-Fernàndez et al. (2013) found that approximately 70% of the AMIGA galaxies meet the Karachentseva criteria for isolation. For these iETGs, this number is 63 ± 10% (the error is due to galaxies without data). About half of the iETGs do not pass the strictest test, but are still expected to be only minimally affected by any neighbours (except possibly KIG 595, those with missing data, and the two conflicts with Verley et al. 2007a).

We conclude that the our iETG sample is consistent with the level of isolation in the KIG population as a whole, and they mostly fulfil the Q and η criteria for isolation. We consider the galaxy sets of Verley et al. (2007a) and Argudo-Fernàndez et al. (2013), which differ in their isolation criteria, in the discussion.

3. Observations, data reduction, and analysis

3.1. Observations

Observations have been performed during a single run from April 9 to April 15, 2018, at the 1.8 m VATT. Photometric conditions varied greatly: the night of 12 April was lost, as were parts of some other nights. We used the back-illuminated 4K CCD (STA0500A), which was installed in March 2017 and was updated on October 8, 2017. The full well is about 117 000 e$^-$, limited by the ADC (16 bit, 65536 DN). The readout noise is 3.9 e$^-$ rms and the gain is 1.8 e$^-$ ADU^{-1}. The number of pixels is 4096 × 4096 (15 × 15 microns) for a total field of view (FOV) of 12.′5 arcmin square with a pixel scale of 0.′′188/px. The galaxies were observed in the g and r SDSS filters with a binning of 2 × 2 (0.′′376/px) of the images. The observation log is reported in Table 3.

In each band, short multiple exposures of single objects were obtained in order to avoid the saturation of the galaxy centre and strong stellar ghosts in the field, and to properly remove cosmic

Table 2. KIG relevant geometric and photometric properties.

KIG	Other ID	ϵ	PA [deg]	d_{25} [arcsec]	g_T [ABmag]	r_T [ABmag]	NUV$_T$ [ABmag]	$E(B-V)$ [ABmag]	A_r(SDSS) [ABmag]
264		0.26 ± 0.08	95.6	38.83	14.81	14.09	19.30 ± 0.03	0.033	0.077
378	IC 569	0.28 ± 0.13	164.5	47.66	14.99	14.13	20.67 ± 0.16	0.022	0.052
412		0.03 ± 0.06	...	25.01	15.55	14.72	20.21 ± 0.12	0.016	0.037
481	NGC 3682	0.37 ± 0.12	93.3	134.01	12.66	11.94	15.77 ± 0.02	0.080	0.020
490		0.29 ± 0.09	36.3	43.47	14.60	13.83	19.52 ± 0.15	0.024	0.056
517		0.34 ± 0.10	65.9	37.68	14.98	14.13	20.17 ± 0.21	0.018	0.042
578	IC 862	0.00 ± 0.09	...	23.29	15.13	14.26	19.78 ± 0.15	0.019	0.051
595	UGC 8649	0.44 ± 0.11	50.8	93.57	14.29	13.45	19.41 ± 0.11	0.013	0.034
599		0.13 ± 0.07	94.6	64.14	14.14	13.37	19.31 ± 0.13	0.010	0.027
620		0.48 ± 0.19	4.4	35.41	14.91	14.15	18.14 ± 0.04	0.006	0.015
636		0.17 ± 0.07	116.8	35.25	15.03	14.19	20.14 ± 0.06	0.08	0.020
637	NGC 5687	0.43 ± 0.19	103.3	144.59	12.98	12.19	17.20 ± 0.01	0.010	0.026
644		0.59 ± 0.25	85.9	55.23	14.77	13.95	19.74 ± 0.10	0.017	0.044
670		0.41 ± 0.14	148.0	62.83	14.59	13.78	20.57 ± 0.21	0.020	0.051
685		0.14 ± 0.08	110.6	39.28	15.41	14.56	20.87 ± 0.18	0.009	0.024
705	I Zw 126	0.03 ± 0.05	...	36.66	14.57	13.81	18.38 ± 0.06	0.017	0.044
722		0.27 ± 0.14	94.2	63.26	14.15	13.29	...	...	...
732	IC 1211	0.07 ± 0.05	...	80.38	13.27	12.42	18.64 ± 0.08	0.020	0.053
733		0.50 ± 0.18	165.2	53.11	14.49	13.65	19.10 ± 0.11	0.086	0.223
841	NGC 6524	0.39 ± 0.09	156.0	97.53	13.36	12.52	16.78 ± 0.02	0.035	0.090

Notes. Ellipticity, position angle (measured NE), and the isophotal diameter at $\mu_B = 25$ mag arcsec^{-2} are from Jones et al. (2018) (Cols. 3, 4 and 5). Total g, r and NUV integrated magnitudes are reported from NED. The errors reported in NED for SDSS magnitudes (CModel) are of about 0.002–0.003 mag.

rays. Column 2 reports the total integration time. A pipeline was developed for bias and dark subtraction to create a master flat in each band for image correction before the final images were registered and co-added. While the bias and dark corrections are standard, the flat-fielding was performed by preparing an `autoflat` procedure. It consists of an accurate masking of all sources in the images, which were stacked after normalisation. For the masking we used `Noisechisel` (Akhlaghi & Ichikawa 2015). This final co-added image is the master flat that we applied to single images in each band. After bias, dark, and flat-field corrections, the images were finally registered for astrometry and co-added using `SWarp` (Bertin et al. 2002). Unfortunately, the flat fielding is not able to completely eliminate certain artefacts, such as dust spots on the filters, because the filter wheel is instable and the filters were frequently changed between exposures. This is identified and masked in the image analysis.

For each image, Col. 5 in Table 3 lists the average Gaussian stellar full width at half-maximum (FWHM) measured with the `IRAF` task `IMEXAMINE`. The measure was performed on stars nearby the galaxy. Figure 3 shows the 2D map of the FWHM variation across the FOV of KIG 264. There is optical distortion towards the outskirts of the CCD fields. However, the plot shows no significant geometric distortions where the galaxy is located. One direct comparison can be made using KIG 685, which was observed by Rampazzo et al. (2019, see their Table 3) with adaptive optics at the LBT. The ellipticity measured by these authors in K band is 0.16 ± 0.05, which is well comparable within the errors with the values of 0.18 ± 0.05 for the bulge that dominates the light profile ($B/T = 0.74$) in both bands. This observing position on the CCD was maintained for all galaxies during the run. A few nearby very extended galaxies fell into the gap between the two CCDs.

3.2. Data reduction

The photometric calibration, the point spread function (PSF) study and the surface photometric analysis were performed using Astronomical Image Decomposition and Analysis (`AIDA`) by Uslenghi & Falomo (2011). This software package, written in `IDL` (Image Display Language), was originally designed to analyse images of galaxies with a bright nucleus and to decompose them into the nuclear and galaxy components. `AIDA` includes tools for PSF characterisation.

Because of the photometric instability and owing to the full-sky coverage of the SDSS survey (York 2000), we corrected the calibration of our g- and r-band images by comparing the photometry of stars in each field with their SDSS magnitudes. Using the SDSS navigator tool, we inspected each target field and identified a set of stars nearby the galaxy. We bootstrapped our instrumental magnitude of these isolated unsaturated stars to their corresponding g and r SDSS magnitude in the star catalogue. The instrumental stellar magnitude in `AIDA` was calculated within different apertures in order to include the entire star, while the nearby residual sky was calculated in a ring cleaned from possible faint nearby stars and objects. The adopted zero-points (ZPs hereafter) and their errors, reported in Col. 6 of Table 3, are the average values and the standard deviation of the scatter in magnitude of the set of stars used.

The PSF shape was obtained from the same set of stars for each g and r field. `AIDA` characterises the PSF using 2D models (both analytical and empirical, or a combination of them), even when they are variable in the FOV. PSF models can be provided by the user or modelled by `AIDA` itself using reference stars in the images. Figure 4 shows one of the stars we used to obtain the PSF in the analysis of KIG 264. Although characterisations of PSF models exist (three Gaussians plus an exponential) up to

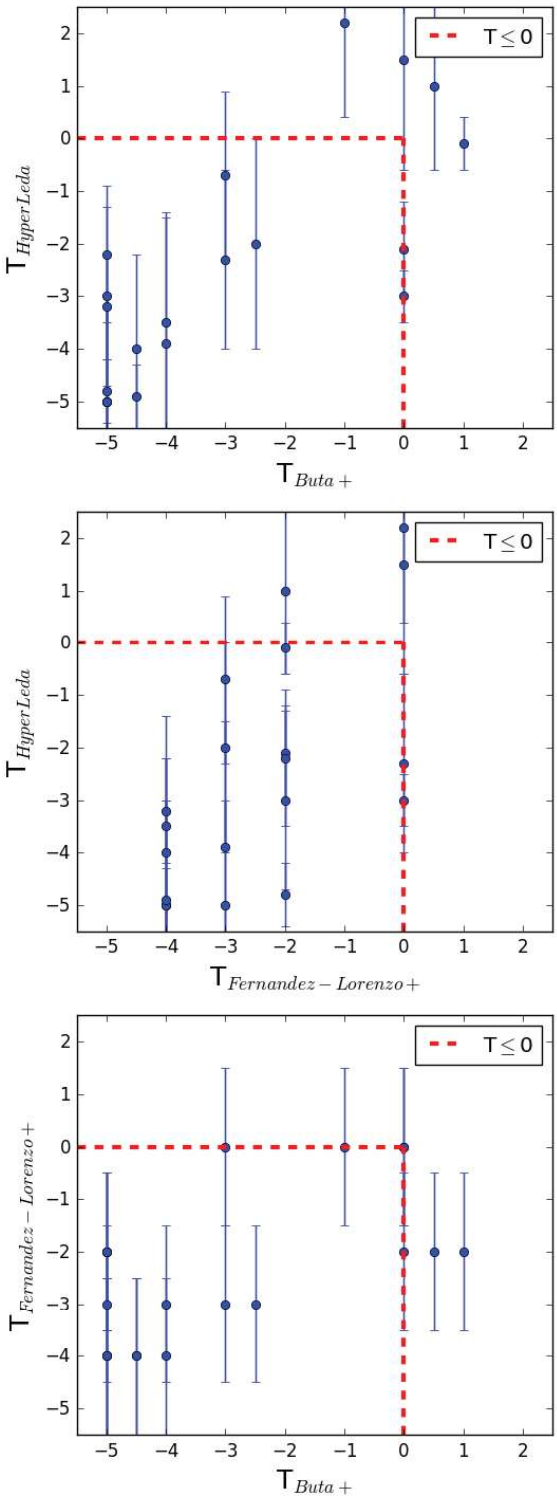

Fig. 1. Comparison between the three classifications into morphological type provided in Table 1. The dashed red rectangle encloses iETGs ($T \leq 0$) in the RC3 classification. Comparisons are made between HyperLeda vs. Buta et al. (2019) (*top panel*), HyperLeda vs. Fernandez-Lorenzo et al. (2012) (*middle panel*), and Buta et al. (2019) vs. Fernandez-Lorenzo et al. (2012) (*bottom panel*).

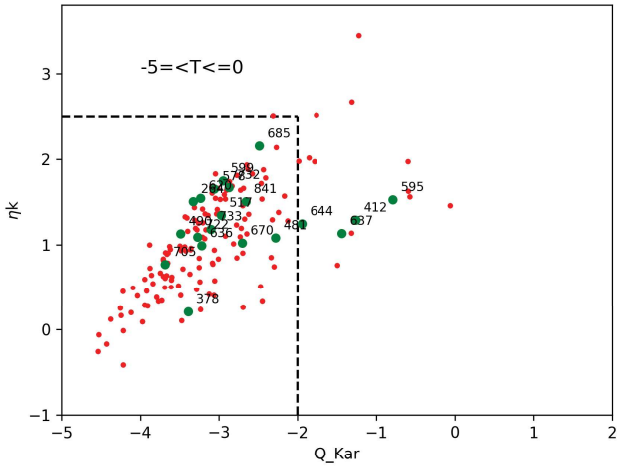

Fig. 2. Degree of isolation of the observed sample (green circles) overplotted on all iETGs (red circles) in the AMIGA sample. According to Verley et al. (2007a), the horizontal and vertical dashed lines enclose the fiducial range of isolated galaxies in the AMIGA sample.

large radii (several arcminutes; Slater et al. 2009; Sandin 2014; Trujillo & Fliri 2016; Karabal et al. 2017; Infante-Sainz et al. 2020, the relatively small extent of our targets means that the analytical PSF model that is adapted is indeed extended to the galaxy outskirts to obtain seeing-corrected parameters (Sandin 2015).

For target galaxies, as in the case of stars, the residual sky background was determined within a ring of variable radius, well outside the galaxy and its peculiar outskirts, masking sources within it. Only a few very extended galaxies are crossed by the CCD gap. This latter was masked during the reduction and analysis procedure. The sky background value was obtained as the average of sectors of the ring, and the errors are the standard deviation of averages. `AIDA` also provides the radial light profile, with associated measurement errors, of the objects. The radial profile is computed by averaging the signal within concentric rings centred on the galaxy. The standard deviation in the rings is then used to evaluate the error bars, after adding in quadrature the uncertainty on the sky background.

In the 2D approach (see also `GALFIT` by Peng et al. 2010 or `IMFIT` by Erwing 2015), all pixels, except for the masked pixels, contribute to the fitting process of the galaxy luminosity distribution, but suffer from the fact that the components have single fixed values for the ellipticity, position angle, and Fourier moments. The information about the variation with radius of the ellipticity, position angle, and isophotal shape parameters obtained from the analysis of the galaxy azimuthal luminosity profile (see e.g. Jedrzejewski 1987) is lost. In modelling the galaxy light profile, `AIDA` adopts two values of the ellipticity and position angle in the case of a bulge plus disc (B+D) decomposition. Before the analysis of our target galaxies, the masking of the foreground and background objects superposed on the target galaxy was also performed manually, that is, masks were tailored to the extension of the objects that were to be removed. The fitting algorithms used by `AIDA` are `MPFIT` (Markwardt 2008) and a modified version of the IDL standard library function `CURVEFIT`, which uses a gradient-expansion algorithm (based on CURFIT; Bevington 1994). The original algorithm was modified in order to allow boundary constraints on the parameters.